NASA CONTRACTOR REPORT

NASA CR-2591

4.

PREDICTION OF PAYLOAD VIBRATION ENVIRONMENTS BY MECHANICAL ADMITTANCE TEST TECHNIQUES, *FINAL REPORT,*

Daniel D. Kana and Luis M. Vargas

5.

NATIONAL AERONAUTICS AND SPACE ADMINISTRATION • WASHINGTON, D. C. • SEPTEMBER 1975

1. Report No. CR-2591	2. Government Accession No.	3. Recipient's Catalog No.
4. Title and Subtitle PREDICTION OF PAYLOAD VIBRATION ENVIRONMENTS BY MECHANICAL ADMITTANCE TEST TECHNIQUES		5. Report Date September 1975
		6. Performing Organization Code
7. Author(s) Daniel D. Kana and Luis M. Vargas		8. Performing Organization Report No. 02-3689
		10. Work Unit No.
9. Performing Organization Name and Address Southwest Research Institute 8500 Culebra Road San Antonio, TX 78284		11. Contract or Grant No. NAS1-12402
		13. Type of Report and Period Covered Contractor
12. Sponsoring Agency Name and Address National Aeronautics and Space Administration Washington, DC 20546		14. Sponsoring Agency Code
15. Supplementary Notes Final report.		

16. Abstract

    A series of experiments was conducted with simple beam and mass launch vehicle and payload models in order to determine the validity of mechanical admittance/impedance techniques applied to development of improved payload vibration tests. Admittances and impedances were measured from tests of the individual components to form matrices which were combined analytically to allow prediction of responses for the complete system. Results were computed for a transmission matrix approach and an admittance matrix approach. Both a rigid body and a flexible payload model were considered. The results clearly demonstrate that the transmission matrix method is too sensitive to measurement error to be practical for this application, while the pure admittance matrix method produces quite satisfactory results. The effects of various errors on the final results are demonstrated.

17. Key Words (Suggested by Author(s)) Vibration Mechanical admittance Mechanical impedance Dynamic tests Payload dynamics	18. Distribution Statement Unclassified - Unlimited Subject Category 39 Structural Mechanics		
19. Security Classif. (of this report) Unclassified	20. Security Classif. (of this page) Unclassified	21. No. of Pages 40	22. Price* $3.75

*For sale by the National Technical Information Service, Springfield, Virginia 22151

TABLE OF CONTENTS

PREDICTION OF PAYLOAD VIBRATION ENVIRONMENTS
BY MECHANICAL ADMITTANCE TEST TECHNIQUES

by

Daniel D. Kana and Luis M. Vargas

Southwest Research Institute
San Antonio, Texas

SUMMARY

A series of experiments were conducted with simple beam and mass launch vehicle and payload models in order to determine the validity of mechanical admittance/impedance techniques applied to development of improved payload vibration tests. Admittances and impedances were measured from tests of the individual components to form matrices which were combined analytically to allow prediction of responses for the complete system. Results were computed for a transmission matrix approach and an admittance matrix approach. Both a rigid body and a flexible payload model were considered. The results clearly demonstrate that the transmission matrix method is too sensitive to measurement error to be practical for this application, while the pure admittance matrix method produces quite satisfactory results. The effects of various errors on the final results are demonstrated.

I. INTRODUCTION

Present plans call for frequent missions to be flown by the space shuttle to ferry a variety of payloads to and from earth orbit. Each payload is likely to have different dynamic characteristics, and may couple significantly with responses of the orbiter vehicle. Thus, each payload must be qualified to its own tailored anticipated vibration environment, in spite of the fact that all payloads will be flown in the same or similar orbiter vehicles. Furthermore, cost effectiveness requires testing the payload alone, although dynamic interaction with the orbiter must be accounted for at the attach points.

It is apparent that simplicity must be a very necessary ingredient of improved payload vibration test procedures if a reasonably economical approach is to be developed. Nevertheless, the essential difference of each test to be performed cannot be overlooked. Therefore, the application of mechanical admittance/impedance concepts in the development of test specifications has been considered as a possible means of achieving some measure of simplicity. That is, characteristics of the orbiter alone will not change from flight to flight, although those of the payloads will. Therefore, if appropriate admittances for the payload and orbiter are determined from tests of each component individually, the results can be combined analytically to allow prediction of the payload environments for various flight operations. Thus, only one test series need be run for the orbiter, although each payload must be investigated individually. Nevertheless, the combined environment can be predicted for all payload/orbiter combinations.

The application of admittance techniques to the problem at hand appears to be relatively straightforward. However, from previous experience it is known that admittance/impedance parameters vary over several orders of magnitude in complex structures, and measurement errors can have a significant influence on results predicted for the combined system. Therefore, the purpose of the program described herein has been to test the validity of this approach on a relatively simple orbiter/payload model. Physical models were built so that admittance tests could be run individually. Sufficient data were measured to form frequency dependent matrix representations of the component characteristics. These matrices were combined analytically to allow prediction of payload model responses to subsequent orbiter model excitation for the coupled system. Further, tests were then conducted on the combined physical models to provide data for correlation with the predictions.

Thus, the present study includes tests on conceptual physical models which bear little resemblance to an actual space shuttle orbiter or payload. For purpose of analogy, however, hereafter the terminology "orbiter" or

"payload" will be used to describe these simple models. Furthermore, it should be recognized that, although the impetus for this study arose from space shuttle considerations, the methods studied are, of course, applicable to launch vehicles in general. Consequently, the results expand upon earlier work reported by Klosterman,[1]* Flannelly, et al.[2] and others.

From the outset of this program, it was recognized that several sources of measurement error could influence the final results, and also as the program progressed, it became apparent that slight alterations in the approach could yield more useful information. However, all results will be presented as a continuous progression in order to avoid confusion. Thus, two somewhat different analytical methods (transmission matrix and admittance matrix) will be described, although it will be shown that only one provided useful results for this application. Furthermore, two different types of payloads (flexible and rigid body) were utilized in order to get a better insight into effects of measurement errors. We begin with a summary of the analytical techniques, provide a description of the physical apparatus, and then present sample results from which conclusions can be drawn.

---

*Superscript numbers in parentheses refer to references given at the end of this report.

II. ANALYTICAL MODELS

The desired objective is to predict the response of a payload when external excitation is applied to the orbiter. For this, the required method is to utilize mechanical admittance or related response parameter concepts, when the parameters have been determined by experiment. It is recognized that several approaches to this problem are possible, depending on whether impedance, admittance, or transmission matrix methods are used. Initially, a transmission matrix approach will be presented, and then a simpler direct admittance approach will follow.

## A.   Transmission Matrix Formulation

1.   General Equations

This development will follow that originally presented by Rubin,[3] although the notation is somewhat different. The proposed model orbiter/ payload combination is shown in state space in Figure 1. First consider the payload as a separate component and write its response in terms of an admittance matrix as

$$\begin{Bmatrix} A_2 \\ A_2' \end{Bmatrix} = \begin{bmatrix} E_2 & G_2^T \\ G_2 & H_2 \end{bmatrix} \begin{Bmatrix} -F_2 \\ F_2' \end{Bmatrix} \tag{1}$$

where E_2, G_2, and H_2 are submatrices having complex elements, and are formed by partitioning the bracketed complete admittance matrix; A_2, F_2 are acceleration and force vectors, respectively. Note that primed quantities represent the input variables and unprimed quantities the output variables. Also, the subscript 2 refers to the payload, while subscript 1 refers to the orbiter. By normal convention, positive forces are those applied to the terminals in admittance matrix formulations; however, for a transmission matrix, positive forces are applied to the input and by the output. Since a transmission matrix will be derived from the above admittance matrix, a negative sign has been added to the output force vector F_2. Thus, in forming the admittance matrix from experimental data, the forces applied to the structure can all be treated as positive, and the negative sign introduced in Equation (1) will provide the correct sign to elements in the transmission matrix to follow.

A rearward transmission matrix can be obtained from Equation (1) as follows:

F_1', A_1' → | ORBITER (1) | F_1, A_1 F_2', A_2' → | PAYLOAD (2) |

F_2, A_2
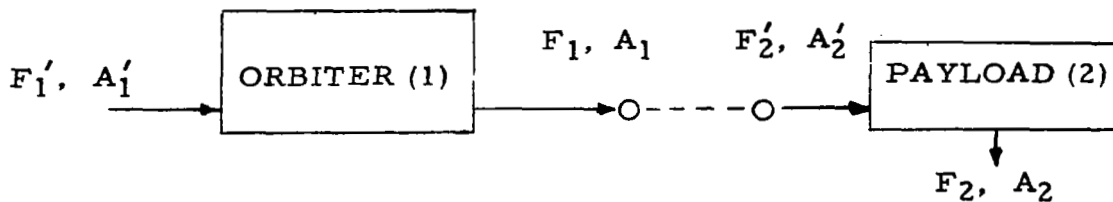
F_1' ~ Excitation forces to orbiter. Assumed known.

A_1' ~ Excitation accelerations to orbiter. Assumed known.

F_1 ~ Output forces on orbiter at payload attach points. Unknown.

A_1 ~ Output accelerations on orbiter at payload attach points. Unknown.

F_2' ~ Input forces to payload at orbiter attach points. Unknown.

A_2' ~ Input accelerations to payload at orbiter attach points. Unknown.

F_2 ~ Response forces at payload. For free response, $F_2 = 0$

A_2 ~ Response accelerations of payload. Unknown.

FIGURE 1. CONCEPTUAL ORBITER/PAYLOAD SYSTEM

$$A_2 = -E_2 F_2 + G_2^T F_2' \tag{2}$$

$$A_2' = -G_2 F_2 + H_2 F_2' \tag{3}$$

From Equation (3), solve for F_2 to obtain

$$G_2^T A_2' = -G_2^T G_2 F_2 + G_2^T H_2 F_2'$$

Note that $G_2^T G_2$ is a square matrix and has an inverse, providing that there are not more outputs than inputs (i.e., G_2 is not a wide matrix). Therefore,

$$\left(G_2^T G_2\right)^{-1} G_2^T A_2' = -F_2 + \left(G_2^T G_2\right)^{-1} G_2^T H_2 F_2' \tag{4}$$

If the left inverse of G_2 is labeled as

$$g_{2\ell} = \left(G_2^T G_2\right)^{-1} G_2^T$$

then from Equation (4) there results

$$F_2 = g_{2\ell} H_2 F_2' - g_{2\ell} A_2' \tag{5}$$

Substituting (5) into (2),

$$A_2 = \left(-E_2 g_{2\ell} H_2 + G_2^T\right) F_2' + E_2 g_{2\ell} A_2' \tag{6}$$

If the number of response points on the payload is less than the number of attach points, then a rearward transmission matrix can be written from Equations (5) and (6) as

$$\begin{Bmatrix} F_2 \\ A_2 \end{Bmatrix} = \begin{bmatrix} J_2 & B_2 \\ C_2 & D_2 \end{bmatrix} \begin{Bmatrix} F_2' \\ A_2' \end{Bmatrix} \tag{7}$$

where

$$J_2 = g_{2\ell} H_2 \qquad\qquad B_2 = -g_{2\ell}$$

$$C_2 = -E_2 g_{2\ell} H_2 + G_2^T \qquad D_2 = E_2 g_{2\ell} \tag{8}$$

6

and recall $g_{2\ell} = \left(G_2^T G_2\right)^{-1} G_2^T$

The restrictions on numbers of response and attach points result from maximum use of information available. For further details, see Reference 3.

Now similarly consider an admittance matrix for the orbiter

$$\begin{Bmatrix} A_1 \\ A_1' \end{Bmatrix} = \begin{bmatrix} E_1 & G_1^T \\ G_1 & H_1 \end{bmatrix} \begin{Bmatrix} -F_1 \\ F_1' \end{Bmatrix} \tag{9}$$

The same steps utilized for the payload yield a rearward transmission matrix for the orbiter:

$$\begin{Bmatrix} F_1 \\ A_1 \end{Bmatrix} = \begin{bmatrix} J_1 & B_1 \\ C_1 & D_1 \end{bmatrix} \begin{Bmatrix} F_1' \\ A_1' \end{Bmatrix} \tag{10}$$

where

$$J_1 = g_{1\ell} H_1 \qquad\qquad B_1 = -g_{1\ell}$$
$$C_1 = -E_1 g_{1\ell} H_1 + G_1^T \qquad D_1 = E_1 g_{1\ell} \tag{11}$$

and

$$g_{1\ell} = \left(G_1^T G_1\right)^{-1} G_1^T$$

The above results can now be combined to predict response for the orbiter/payload combination. For linear structures in series, the combined response can be obtained by the proper combination of the transmission matrices. For rearward transmission matrices

$$\psi = T_q T_{q-1} \cdots T_2 T_1 \psi'$$

where ψ is the state variable at the output

ψ' is the state variable at the input,

and T_q are the rearward transmission matrices.

The response of the payload as a function of the input to the orbiter is thus obtained from Equations (7) and (10) as

$$\begin{Bmatrix} F_2 \\ A_2 \end{Bmatrix} = \begin{bmatrix} J_2 & B_2 \\ C_2 & D_2 \end{bmatrix} \begin{bmatrix} J_1 & B_1 \\ C_1 & D_1 \end{bmatrix} \begin{Bmatrix} F_1' \\ A_1' \end{Bmatrix} \qquad (12)$$

where the output of the orbiter

$$\begin{Bmatrix} F_1 \\ A_1 \end{Bmatrix} \quad \text{from Equation (10) has been}$$

substituted for the input to the payload

$$\begin{Bmatrix} F_2' \\ A_2' \end{Bmatrix} \quad \text{in Equation (7)}$$

Note that F_1 has been equated to F_2' and not to $-F_2'$. While it is true that the $\Sigma F = 0$ at the junction, the formulation of the transmission matrices is such that the output <u>by</u> the terminals of the orbiter, F_1, is positive as is the input <u>to</u> the terminals on the payload, F_2'.

2. <u>Application to Specific Model</u>

For the present study, consider the payload and orbiter configurations shown in Figures 2 and 3, respectively. The payload will have attach or input points 1 - 4, and one output point 5. The output will be free so that $F_5 = 0$. For this case we can write Equation (1) more explicitly as

$$\begin{Bmatrix} a_5 \\ a_1 \\ a_2 \\ a_3 \\ a_4 \end{Bmatrix} = \begin{bmatrix} b_{55} & b_{51} & b_{52} & b_{53} & b_{54} \\ b_{15} & b_{11} & b_{12} & b_{13} & b_{14} \\ b_{25} & b_{21} & b_{22} & b_{23} & b_{24} \\ b_{35} & b_{31} & b_{32} & b_{33} & b_{34} \\ b_{45} & b_{41} & b_{42} & b_{43} & b_{44} \end{bmatrix} \begin{Bmatrix} -f_5 \\ f_1 \\ f_2 \\ f_3 \\ f_4 \end{Bmatrix} \qquad (13)$$

where the acceleration and force components correspond to the coordinate system given in Figure 2. Note that the dashed lines partition the admittance matrix into the form corresponding to that in Equation (1)

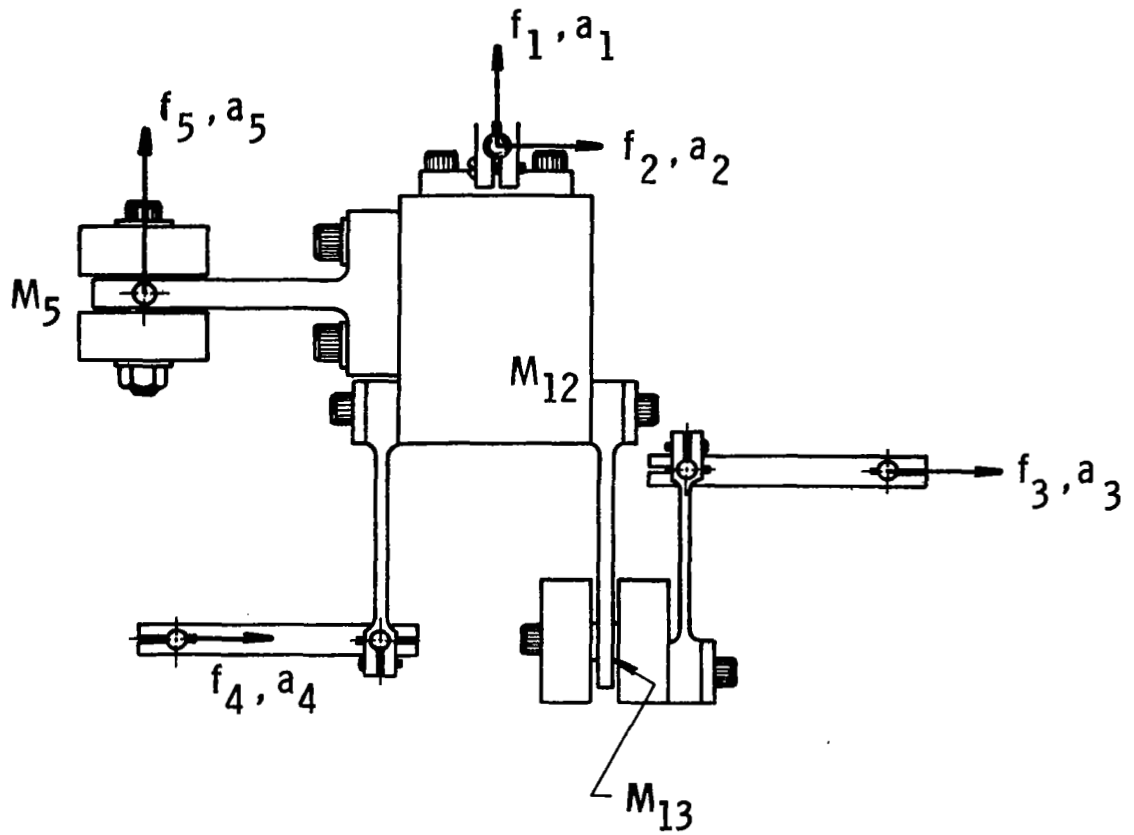Similarly for the orbiter, corresponding to Equation (9) and Figure 3, one can write

Fig. 2. Flexible Payload Model Showing
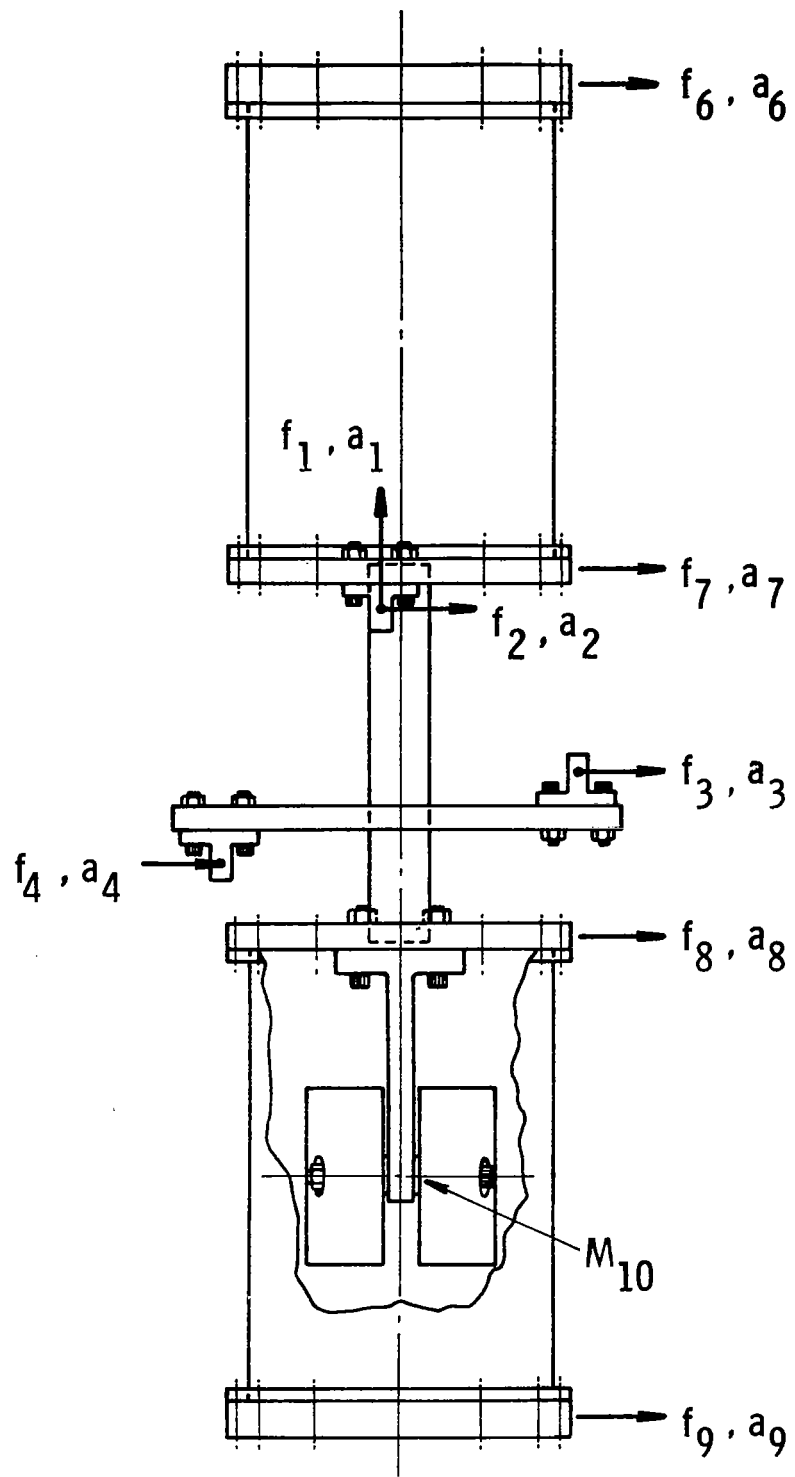Measurement Coordinate System

Fig.3. Orbiter Model Showing Measurement Coordinate System

$$-\begin{Bmatrix} a_1 \\ a_2 \\ a_3 \\ a_4 \\ \hline a_6 \\ a_7 \\ a_8 \\ a_9 \end{Bmatrix} = -\left[\begin{array}{cccc|cccc} c_{11} & c_{12} & c_{13} & c_{14} & c_{16} & c_{17} & c_{18} & c_{19} \\ c_{21} & c_{22} & c_{23} & c_{24} & c_{26} & c_{27} & c_{28} & c_{29} \\ c_{31} & c_{32} & c_{33} & c_{34} & c_{36} & c_{37} & c_{38} & c_{39} \\ c_{41} & c_{42} & c_{43} & c_{44} & c_{46} & c_{47} & c_{48} & c_{49} \\ \hline c_{61} & c_{62} & c_{63} & c_{64} & c_{66} & c_{67} & c_{68} & c_{69} \\ c_{71} & c_{72} & c_{73} & c_{74} & c_{76} & c_{77} & c_{78} & c_{79} \\ c_{81} & c_{82} & c_{83} & c_{84} & c_{86} & c_{87} & c_{88} & c_{89} \\ c_{91} & c_{92} & c_{93} & c_{94} & c_{96} & c_{97} & c_{98} & c_{99} \end{array}\right] \begin{Bmatrix} -f_1 \\ -f_2 \\ -f_3 \\ -f_4 \\ \hline f_6 \\ f_7 \\ f_8 \\ f_9 \end{Bmatrix} \quad\text{---} \quad (14)$$

Note that point 5 does not appear on the orbiter. Again, the dashed lines indicate a partition corresponding to Equation (9).

The procedure for the application of the transmission matrices now becomes clear. The elements of the admittance matrices in Equations (13) and (14) must be measured by experiments on the payload and orbiter individually. Substitution of the values into these matrices then allows subsequent matrix manipulations according to the previously-outlined development. Ultimately, Equation (12) is then used to predict the response of point 5 on the payload to an arbitrary input at points 6, 7, 8, and 9 of the orbiter.

B.   Admittance Matrix Formulation

During the process of applying the above method to the prediction problem, it was discovered that another simpler technique could be utilized. As a result, both methods were studied and the results compared. The second method will be referred to as the admittance matrix method, and will now be described. One development for this method is given in Reference 4. However, here the prediction equation will be derived directly from Equation (12). This development will be applicable only for a case where the payload output force is zero in the coupled system (as is the present case).

Consider $F_2 = 0$ in Equation (12) and perform the indicated matrix multiplications

$$0 = (J_2 J_1 + B_2 C_1) \, F_1' + (J_2 B_1 + B_2 D_1) \, A_1' \tag{15a}$$

$$A_2 = (C_2 J_1 + D_2 C_1) \, F_1' + (C_2 B_1 + D_2 D_1) \, A_1' \tag{15b}$$

Now substitute Equations (8) and (11) into Equation (15a) to obtain

$$\left[g_{2\ell}(H_2 + E_1) \, g_{1\ell} H_1 - g_{2\ell} G_1^T \right] F_1' = g_{2\ell}(H_2 + E_1) \, g_{1\ell} A_1'$$

11

In this equation, multiply on the left by $(H_2+E_1)^{-1} \left(g_{2\ell}^T \; g_{2\ell}\right)^{-1} g_{2\ell}^T$. There results

$$g_{1\ell} A_1' = \left[g_{1\ell} H_1 - (H_2+E_1)^{-1} G_1^T \right] F_1' \qquad (16)$$

Now substitute Equations (8) and (11) into Equation (15b) to obtain

$$A_2 = \left[-E_2 g_{2\ell} (H_2+E_1) g_{1\ell} H_1 + G_2^T g_{1\ell} H_1 + E_2 g_{2\ell} G_1^T \right] F_1'$$

$$+ \left[E_2 g_{2\ell} (H_2+E_1) - G_2^T \right] g_{1\ell} A_1'$$

Into this, substitute Equation (16), perform the matrix multiplication, and clear to obtain

$$A_2 = G_2^T (H_2+E_1)^{-1} G_1^T F_1'$$

Since $A_2 = a_5$ for the present case, this becomes

$$a_5 = G_2^T (H_2+E_1)^{-1} G_1^T F_1' \qquad (17)$$

The above expression becomes the prediction equation for response of point 5 of the payload to excitation of the orbiter at points 6 through 9. Again, elements of the various admittance matrices are measured from experiments on the payload and orbiter individually. Substitution of these values into the admittance matrices then allow matrix manipulations according to Equation (17), whereby the response is predicted. A careful scrutiny of the component matrices of Equation (17) reveals that it requires significantly fewer measurements than does Equation (12), which is the basis for the transmission matrix method.

Although Equation (17) has been derived in terms of admittance parameters, it can also be used if some of the data has been acquired from blocked impedance tests. For example, it may be more feasible to run this type of test on the payload, rather than one with free-free boundary conditions. In this case one would form from the results a 4 X 4 impedance matrix Z_2 for the payload while it was tested alone. Then note that

$$H_2 = Z_2^{-1} \qquad (18)$$

This expression can be combined with Equation (17) to form another prediction method. It is obvious that even other test combinations and procedures are possible, but they were not investigated under the present program.

C. Rigid Body Payload Matrix

It was mentioned previously that two types of payloads were used in the program. The flexible payload was shown in Figure 2. A rigid body payload was also used, and is shown in Figure 4. Only the admittance matrix prediction method (Equation (17)) was applied for this payload. However, use of the rigid body also allowed a convenient analytical representation for the payload admittance matrix that could readily be compared with values measured experimentally. An admittance matrix for a three-dimensional rigid body has been given by Rubin[3]. Thus, referring to Figure 4, the response at point j to a force at point k, i. e., the jk-th element of the 5×5 matrix in Equation (12), is:

$$b_{jk} = \left[W + R_j^T \, J^{-1} \, R_k \right]_{mn} \tag{19}$$

where W is a 3×3 diagonal matrix whose diagonal elements are all equal to the weight of the rigid body, and

$$R_j = \begin{bmatrix} 0 & -z_j & y_j \\ z_j & 0 & -x_j \\ -y_j & x_j & 0 \end{bmatrix}$$

that is, a matrix of coordinates of the response point j relative to the body center of gravity;

$$R_k = \begin{bmatrix} 0 & -z_k & y_k \\ z_k & 0 & -x_k \\ -y_k & x_k & 0 \end{bmatrix}$$

that is, a matrix of coordinates of the excitation point k relative to the body center of gravity; and

$$J = \begin{bmatrix} J_{xx} & -J_{xy} & -J_{xz} \\ -J_{xy} & J_{yy} & -J_{yz} \\ -J_{xz} & -J_{zy} & J_{zz} \end{bmatrix}$$

that is, a matrix of moments and products of inertia for the rigid body. Note that the subscripts mn in Equation (19) emphasize that one must use only that element of the resulting 3×3 matrix that corresponds to
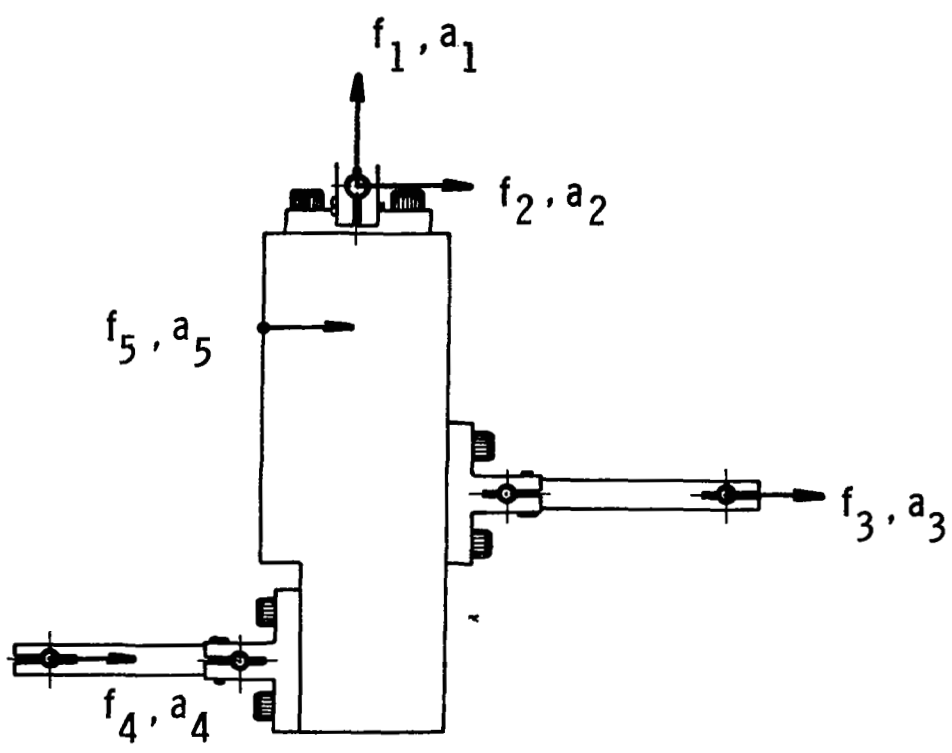
13

Fig. 4. Rigid Payload Model Showing
Measurement Coordinate System

14

the x, y, or z direction of actual force or response used at a given point in Figure 4. Careful study of the rigid body forms will reveal that the admittance matrix must be comprised of real elements that are independent of frequency for this case.

Use of Equation (19) now allows computation of the appropriate elements of the G_2^T and H_2 matrices for use in Equation (17) as a prediction equation. Use of this procedure will be referred to as a theoretical rigid body payload admittance matrix, while use of experimental parameters will be referred to as a measured rigid body payload admittance matrix.

III. DESCRIPTION OF APPARATUS AND PROCEDURES

A description of the physical models, their associated instrumentation, and data acquisition procedures will be given in this section.

A. Orbiter

A schematic of the experimental orbiter model is shown in Figure 3, while a photograph showing the flexible payload installed is shown in Figure 5. The orbiter is symmetrical relative to a central plane parallel to the paper in Figure 3. The model is 69.3 cm (27.25 in.) long and consists of two identical 22.9 cm (9 in.) long cylindrical tanks separated by a center payload section. Each cylindrical tank was rolled from 0.305 mm (0.012 in.) thick 1100-H14 aluminum sheets to an outer diameter of 15.24 cm (6 in.) and butt-welded along the longitudinal seam. Flanges were spot-welded to both ends of each tank, allowing the tanks to be bolted to heavy end plates. The steel end plates were designed to reduce frequencies of the overall bending, torsion, and longitudinal modes into a useful range for making admittance measurements. The center payload section consists of an aluminum payload support ring which is bonded to two plastic bars that form a bending backbone for the model. These bars were made of polyvinyl chloride to provide bending mode damping from 1% to 2% critical. One vertical and three horizontal-acting mounting points were provided for the payload. These mountings were commercially-available flexure pivots so that they behaved as pure pin joints, whereby no moment could be transmitted through them. An additional mass (M_{10}) was supported on a plastic cantilever beam to represent an arbitrary additional elastic degree of freedom of some internal component.

B. Flexible Payload

The flexible payload, as shown in Figure 2, consists of three masses, M_{12}, M_{13}, and M_5 joined by plastic beams, and supported by aluminum links attached to the aluminum ring of the center section. Both masses M_{12} and M_{13} are made of steel while mass M_5 is made of lead. Flexural pivot pins were used at attach points 1, 2, 3, and 4 to insure that loads perpendicular to one of the attach points would be transmitted faithfully without any moment being produced, as mentioned previously. For the blocked impedance test, minor redesign to the attachment for points 1 and 2 was necessary. A double pin or yoke attachment was used at the joint so that the 1-direction was fixed independently of the 2-direction. More information on the link arrangement will be given later.

16

C.   Rigid Body Payload

A rigid payload model, as shown in Figure 4, was designed to be used in a series of admittance tests. The steel rigid payload model has overall dimensions of 6.4 x 5.6 x 13.3 cm (2.52 x 2.2 x 5.25 in.). Aluminum brackets and support links were used as with the flexible payload model. Dimensions were adjusted so that the interface or attach points between the orbiter and rigid payload would be the same as the interface points between the orbiter and flexible payload.

D.   Admittance Tests

The admittance tests consisted of acquiring steady-state sinusoidal response data from which mechanical admittance values could be computed for a given component or system. The item was suspended in a low frequency support in order to simulate a free-free configuration. Figure 5 shows a photograph of the orbiter with flexible payload installed. Small piezoelectric accelerometers were used to measure responses at the designated points, while a constant force excitation signal was applied by a light electromagnetic coil. The exciter coil was capable of excitation down to DC in frequency, and force was calibrated in terms of the armature current. An input accelerometer ring was used to avoid excitation directly through the accelerometer at this point. This ring was bolted to the input point before the accelerometer was mounted inside it. This arrangement avoided distortion of input acceleration signals. Figure 6 shows the arrangement used for the flexible payload. It can be seen that various stabilizers or guides were also used as part of the suspension system. Rubber bands were used for this purpose. Also, for the case of the payloads, ballast weights were used at each attach point. Each ballast was set at exactly the weight of the small coil plus its connecting link so that all excitation point mass values were properly accounted for.

Data acquisition was performed by the instrumentation system shown in block diagram form in Figure 7. Initially, sine sweeps of constant force amplitude applied at one point were conducted and responses at selected points were recorded on an X-Y plotter. In order to obtain a good signal to noise ratio both input and output were filtered through tracking filters having two-hertz bandwidths. The signal was subsequently passed through a log converter in order to allow plotting of signals having a wide dynamic range. After initial tests, admittance data were taken at certain selected discrete frequencies. Both real and imaginary (CO and QUAD) values of admittance were read after being computed by the CO/QUAD analyzer. The data were read visually from a digital voltmeter, and later keypunched into input format for a digital computer. Overall accuracy available with this system was estimated at 5% to 10% maximum error.
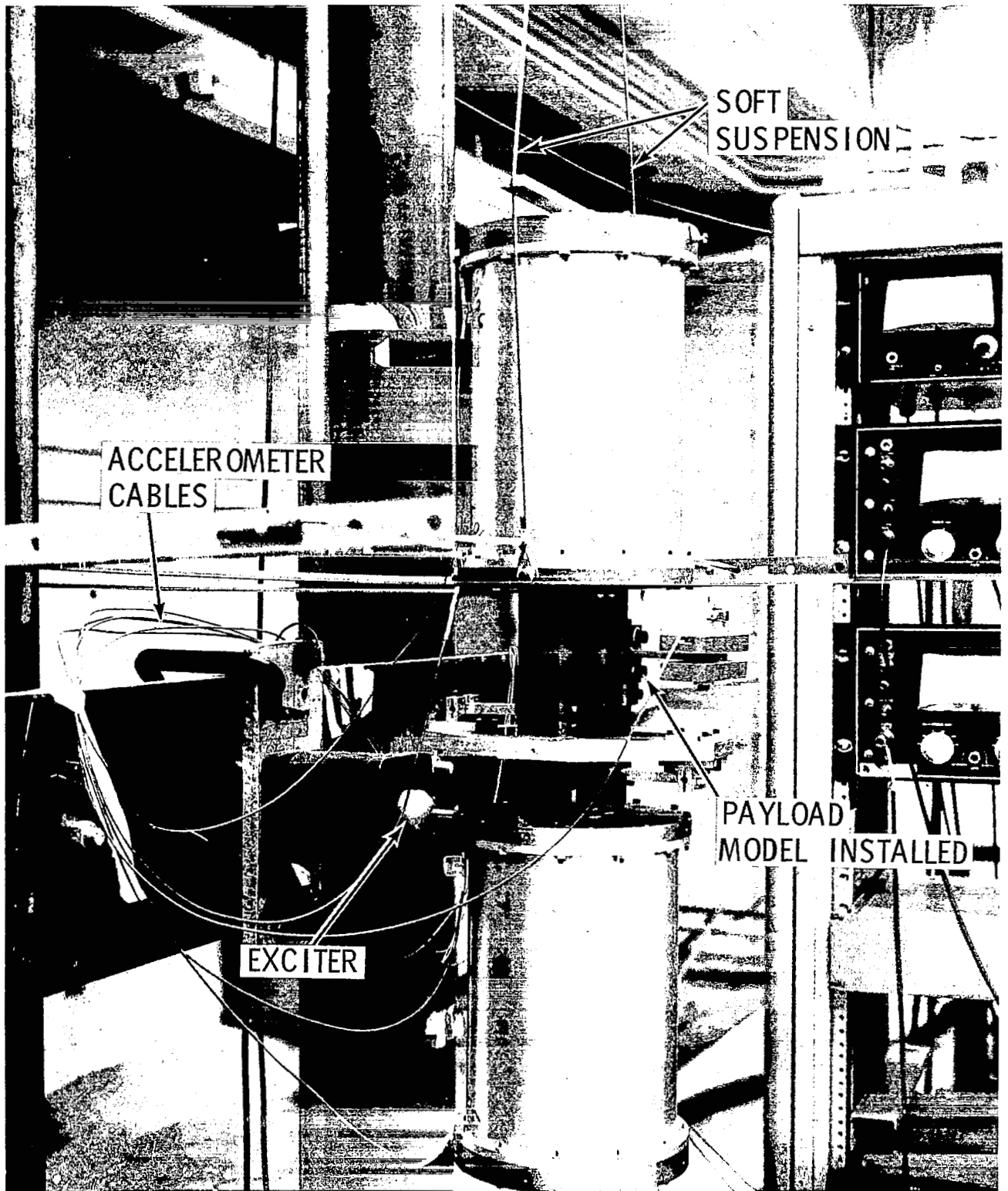
Fig. 5. Freely-Supported Test Configuration of
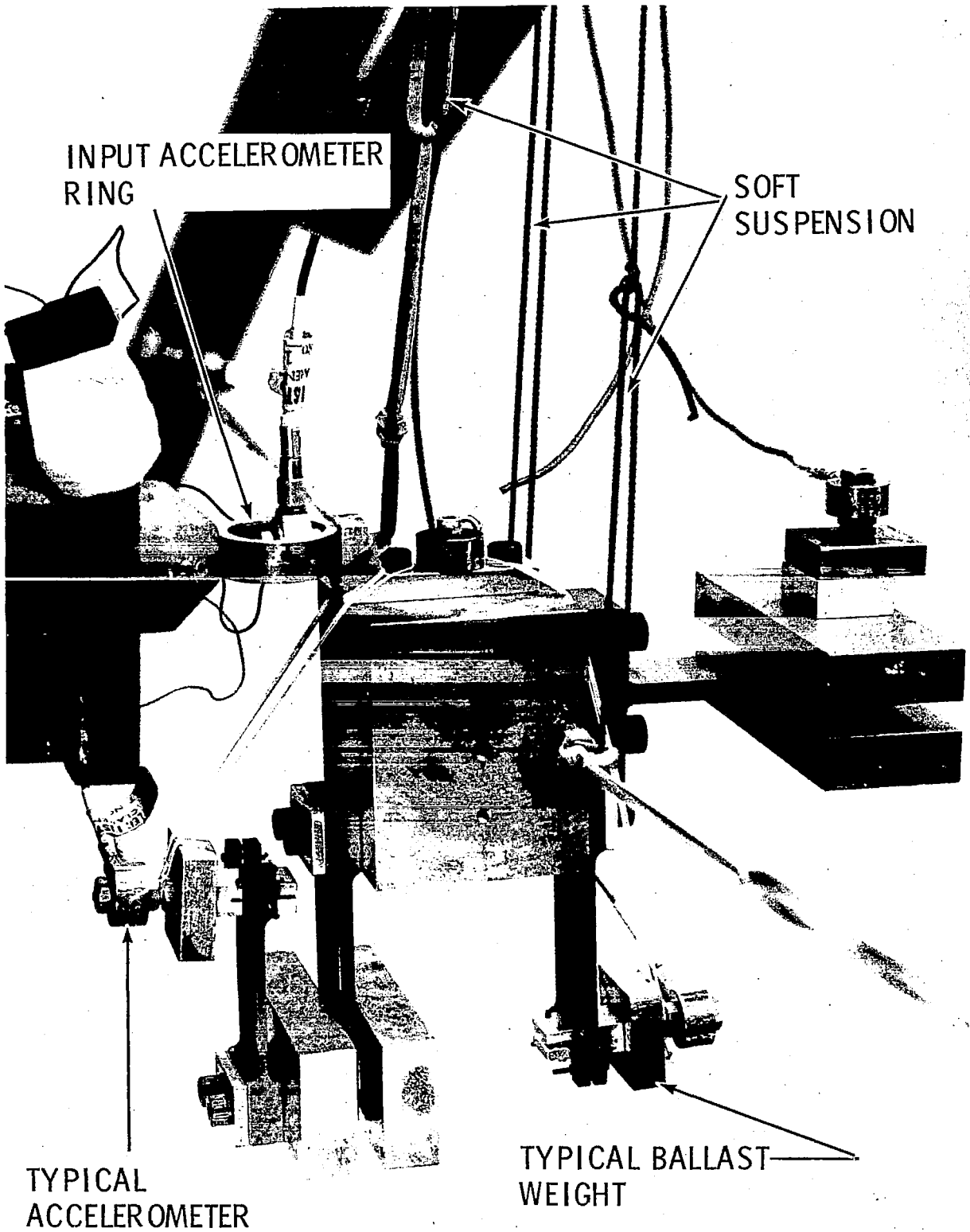Orbiter Model with Flexible Payload

INPUT ACCELEROMETER RING

SOFT SUSPENSION

TYPICAL ACCELEROMETER

TYPICAL BALLAST WEIGHT

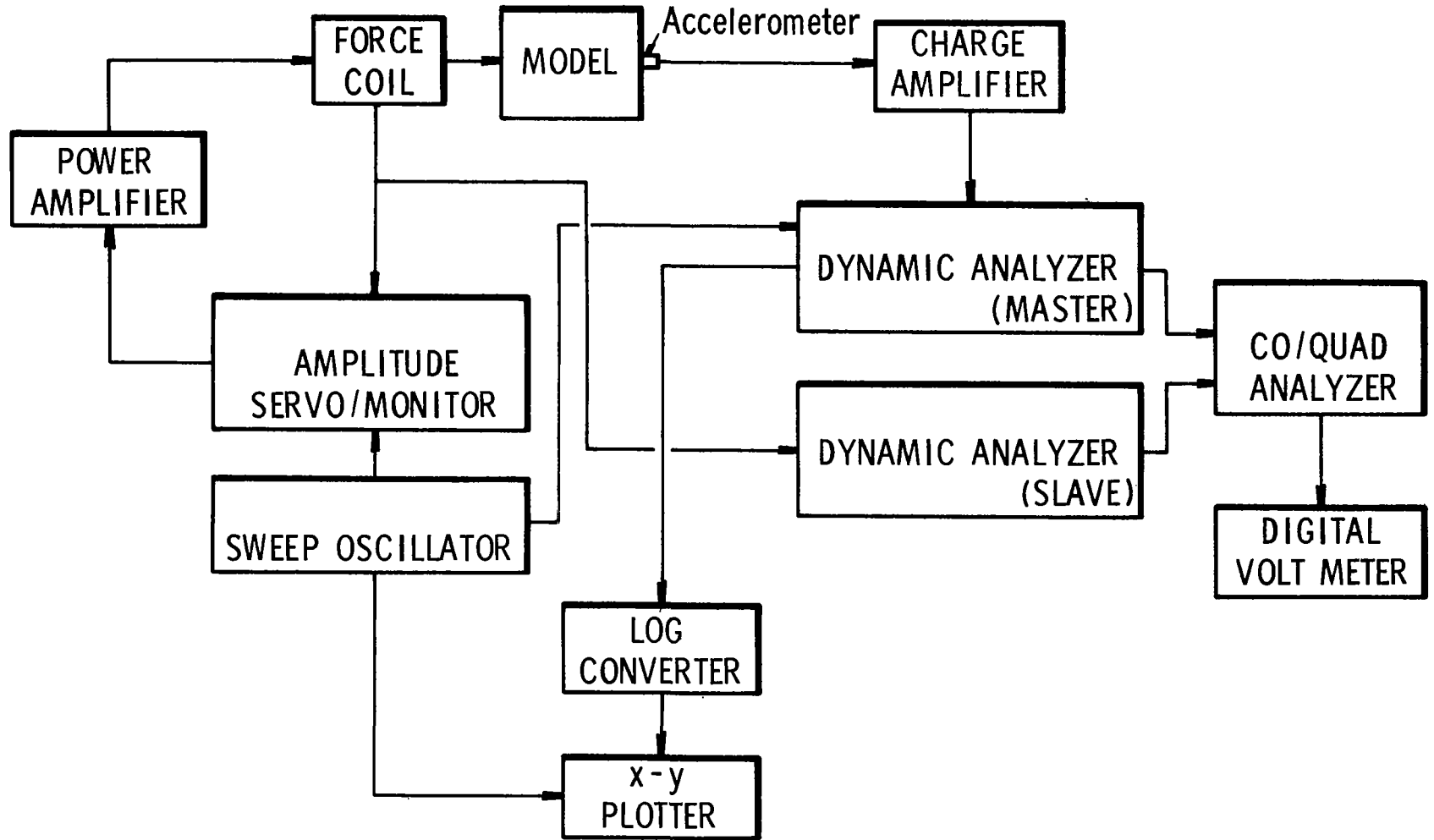Fig. 6. Admittance Test of Flexible Payload

19

Figure 7. Block Diagram of Instrumentation for Admittance Measurements

A typical test sequence for the combined system, flexible payload, and orbiter is given in Table I. Initially, the combined system with flexible payload installed was tested in order to obtain optimum frequencies at which subsequent data would be acquired. (This procedure was followed in order to reduce the number of measurements required for this study and could not normally be applied in practice.) Since all parameters were frequency-dependent, it is obvious that subsequent measurements performed for different set-up positions had to be made at exactly the same frequencies. Thus, the twenty discrete frequencies indicated were chosen as a good representation of resonance, antiresonance, and between-resonance frequencies. It was also decided that the results of Step II for the combined system (i.e., a_5/f_8, with f_6, f_7, $f_9 = 0$) would be chosen as the response with which to compare subsequent predicted values.

Steps III and IV in Table I describe the sequence used for acquiring the admittance data for these components. Note that each case required a different setup for the excitation coil, and data had to be acquired for each of the twenty frequencies for each setup. Obviously, a large volume of data were necessary for the indicated procedure which was applicable to the transmission matrix method. Significantly fewer measurements were necessary for application of the admittance matrix method, as can be seen from a careful study of the dimension of the matrices derived for that method.

A suspension similar to that shown in Figure 5 was also used for admittance testing of the system with the rigid body payload installed. Also, an arrangement similar to that of Figure 6 was used to test the rigid body payload for its admittance parameters. Correspondingly, procedures similar to those outlined in Steps II and III of Table I were used for the system and payload tests, respectively.

E.   Blocked Impedance Tests

A blocked impedance test was performed on the flexible payload only. It was felt that responses for this condition may be more like those of the payload installed in the orbiter, and increased prediction accuracy might therefore result. Some modification of the connecting links were necessary in order to attach the payload at points 1 and 2 independently. That is, the payload was attached in the 1-direction independently of the 2-direction. This was accomplished by use of a double pin at the joint. Also, the payload was mounted to a massive rigid fixture through very stiff piezoelectric force transducers which did not allow motion at the blocked points. One attachment point was left free and the small exciter along with an accelerometer were attached. Some of these details are apparent in Figures 8 and 9.

TABLE I

TEST SEQUENCE FOR SYSTEM
WITH FLEXIBLE PAYLOAD

I. General

Steady-state sinusoidal acceleration responses are obtained for a single fixed amplitude forced response as outlined below. Data are taken at each of the following frequencies:

5.0,   10.0, 10.9^{*} 12.0,   15.0, 16.8^{**} 19.0, 20.3^{*}

21.5^{*} 23.0, 24.3^{*} 27.0,   29.0, 31.0^{*} 32.0,   37.0,

45.0 47.6^{*} 50.0,   60.0 — Hz.

* Resonance frequencies for combined system.

** Antiresonance frequencies for combined system.

II. Combined System

A. Excite at f_8, read accelerations a_5, a_6, a_7, a_8, a_9

III. Flexible Payload

A. Excite at f_1, read accelerations a_1, a_2, a_3, a_4, a_5
B. Excite at f_2, "   "   "
C. Excite at f_3, "   "   "
D. Excite at f_4, "   "   "
E. Excite at f_5, "   "   "

IV. Orbiter

A. Excite at f_1, read accelerations a_1, a_2, a_3, a_4, a_6, a_7, a_8, a_9
B. Excite at f_2, "   "   "   "
C. Excite at f_3, "   "   "   "
D. Excite at f_4, "   "   "   "
E. Excite at f_6, "   "   "   "
F. Excite at f_7, "   "   "   "
G. Excite at f_8, "   "   "   "
H. Excite at f_9, "   "   "   "

NOTE: Coordinate system for above parameters defined in Figures 2 and 3.
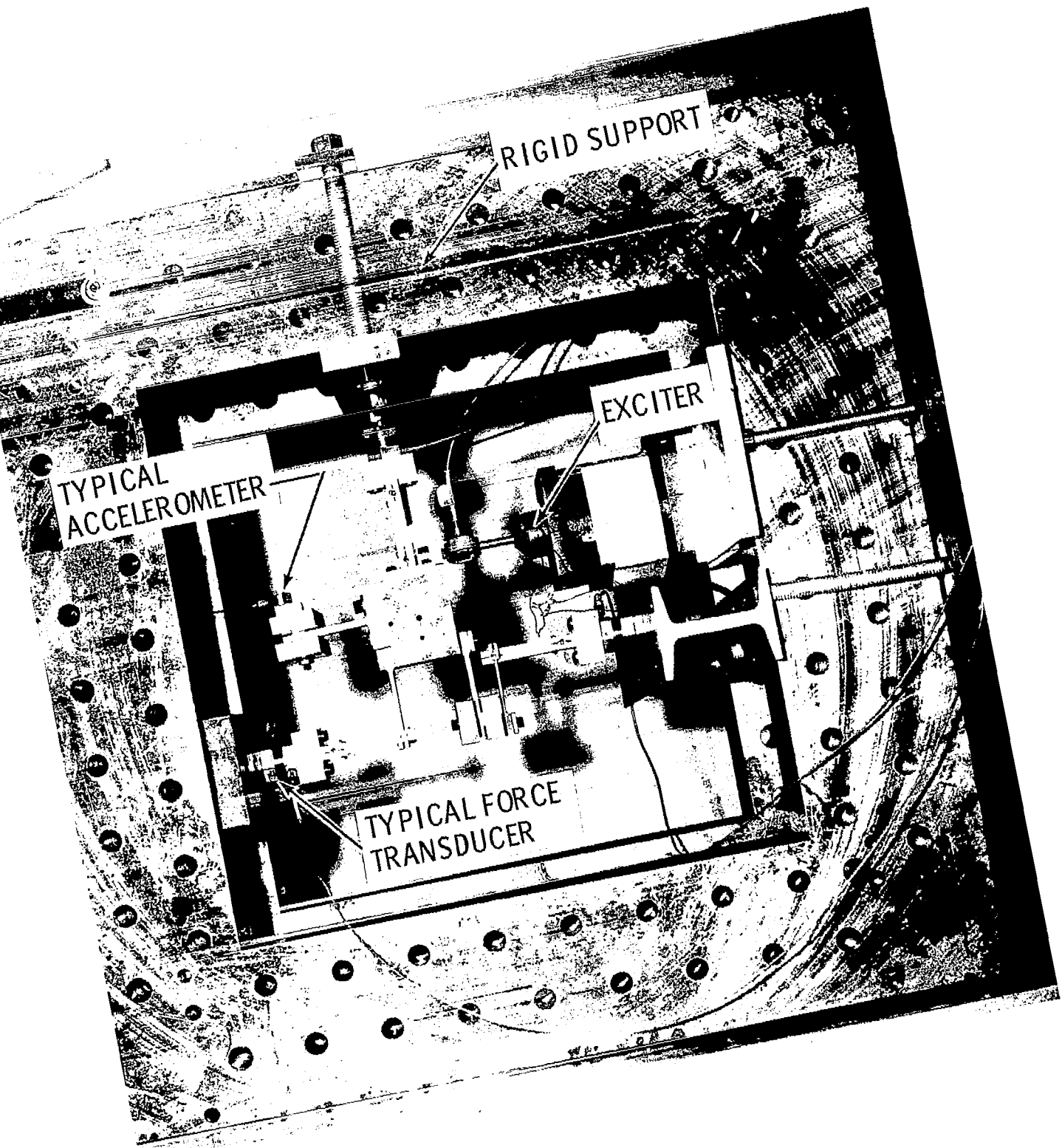
Fig. 8. Overall View of Blocked Impedance
Test of Flexible Payload
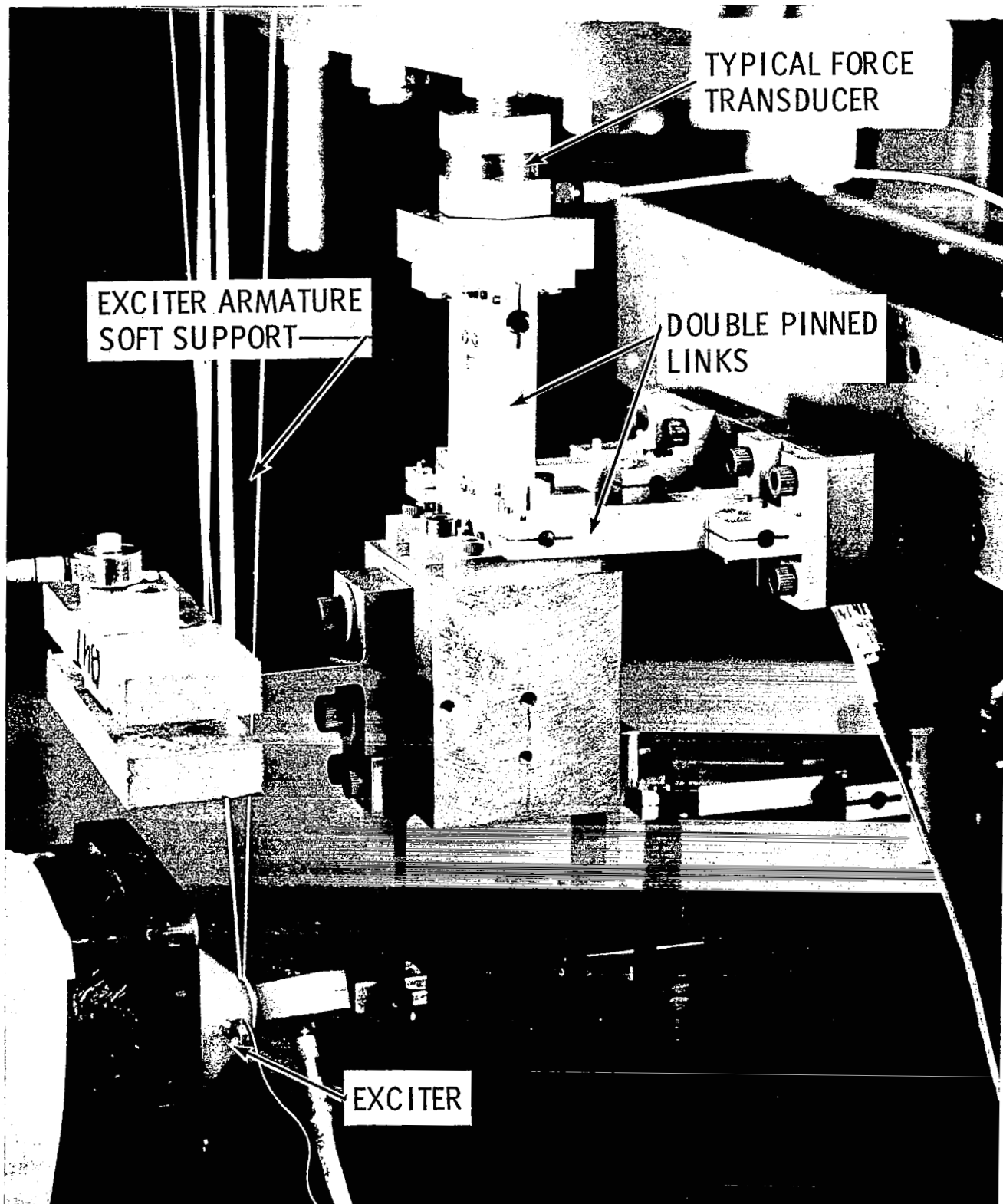(Excitation at Point 2)

Fig. 9.   Blocked Impedance Test of Flexible Payload
(Excitation at Point 4)

For these tests, the input acceleration was maintained constant and the resultant forces at the input and the three other response points were recorded. Measurements were made at each of the discrete frequencies previously used for the admittance tests. As in the admittance tests, the force signals and the constant acceleration were filtered, then input to the CO/QUAD analyzer to compute real and imaginary parts of the complex impedances.

IV. ANALYTICAL AND EXPERIMENTAL RESULTS

A.   Transmission Matrix Formulation

Sample results for magnitudes of acceleration admittances are shown in Figures 10 and 11 for the orbiter and flexible payload, respectively. Similar curves were obtained for excitation at all other points on each component. Numerical values for the complex admittances read at each of the discrete frequencies listed in Table I will not be tabulated for brevity sake. Rather, final results will be given in terms of a comparison of measured and predicted values on similar frequency response plots.

Several comments will be made about the sample results in Figures 10 and 11. For the orbiter, two strong resonances occur in the frequency range up to 60 Hz. The first represents the coupled resonance of the internal mass M_{10} at about 21 Hz, and the second is the first overall bending mode at about 34 Hz. Four major resonances occur for the payload, as seen in Figure 11, and are identified with a mass that experiences the strongest motion. Those identified as Input 3 and Input 4, are associated with those corresponding points, although no specific identification was given to the effective mass at those points. An immediate conclusion from these figures is that the admittance parameters vary considerably over several orders of magnitude.

Final results for the transmission matrix formulation are shown in Figure 12, where experimental and predicted results are identified. Computed predictions were finally obtained at nineteen different frequencies identified in Table I (60 Hz was omitted because of electrical noise problems). The predicted points identified as "transmission matrix" were obtained from use of "as measured" admittances, which resulted in some nonsymmetry in the admittance matrices. This was considered to be measurement error, and a second set of results, identified as "average transmission matrix," was computed by averaging the corresponding off-diagonal matrix elements and using the resulting symmetrical matrices in the computations. In either case, however, it is obvious that the correspondence between predicted and measured response is very poor, although the qualitative shape of the curve is apparent. Repeated attempts were conducted to determine whether the wide discrepancy was caused by programming error. No such error was discovered. The final conclusion reached was that the error is genuinely inherent in the use of the transmission matrix method, although the fact that essentially all results were too large did seem peculiar.
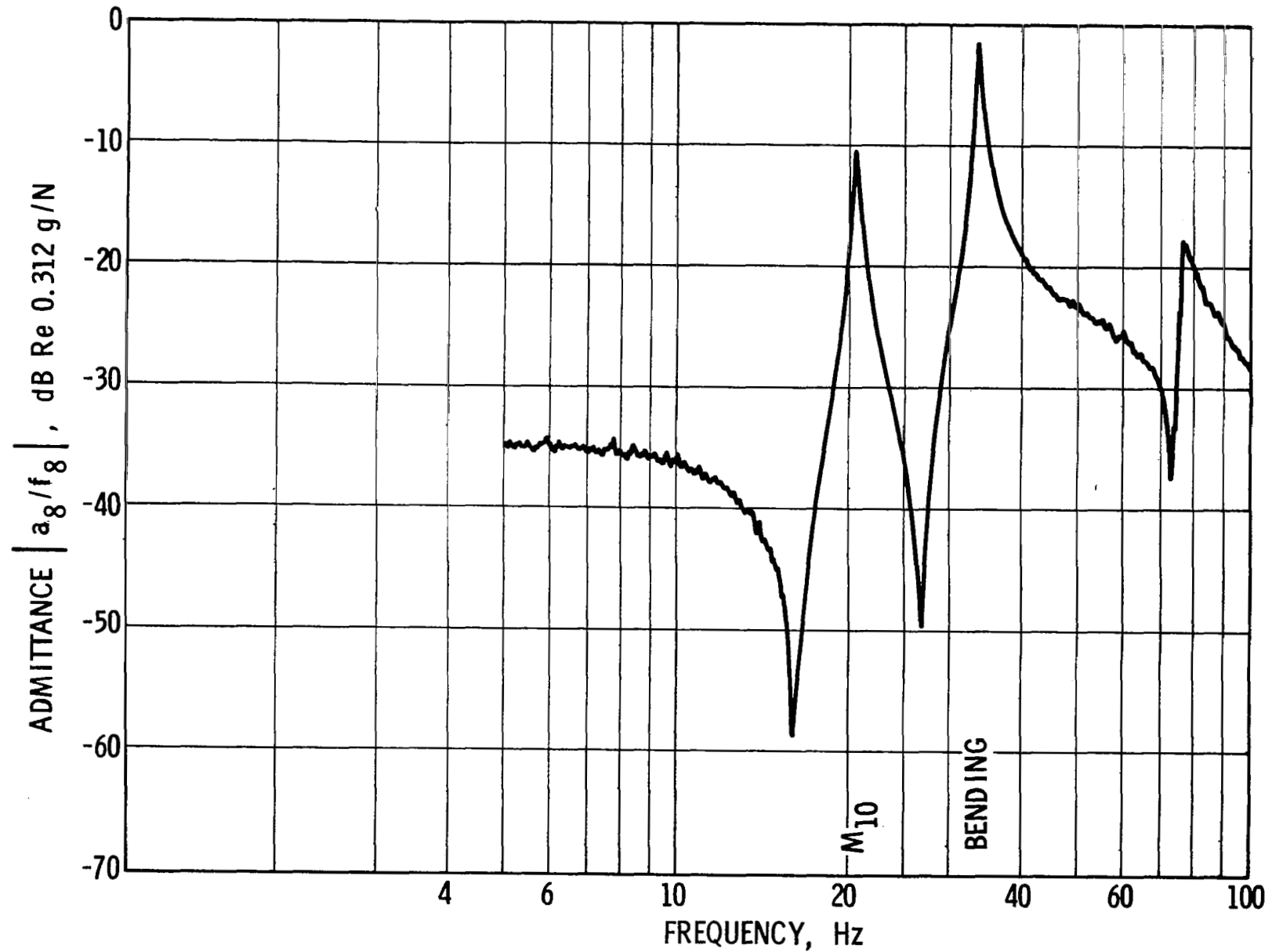
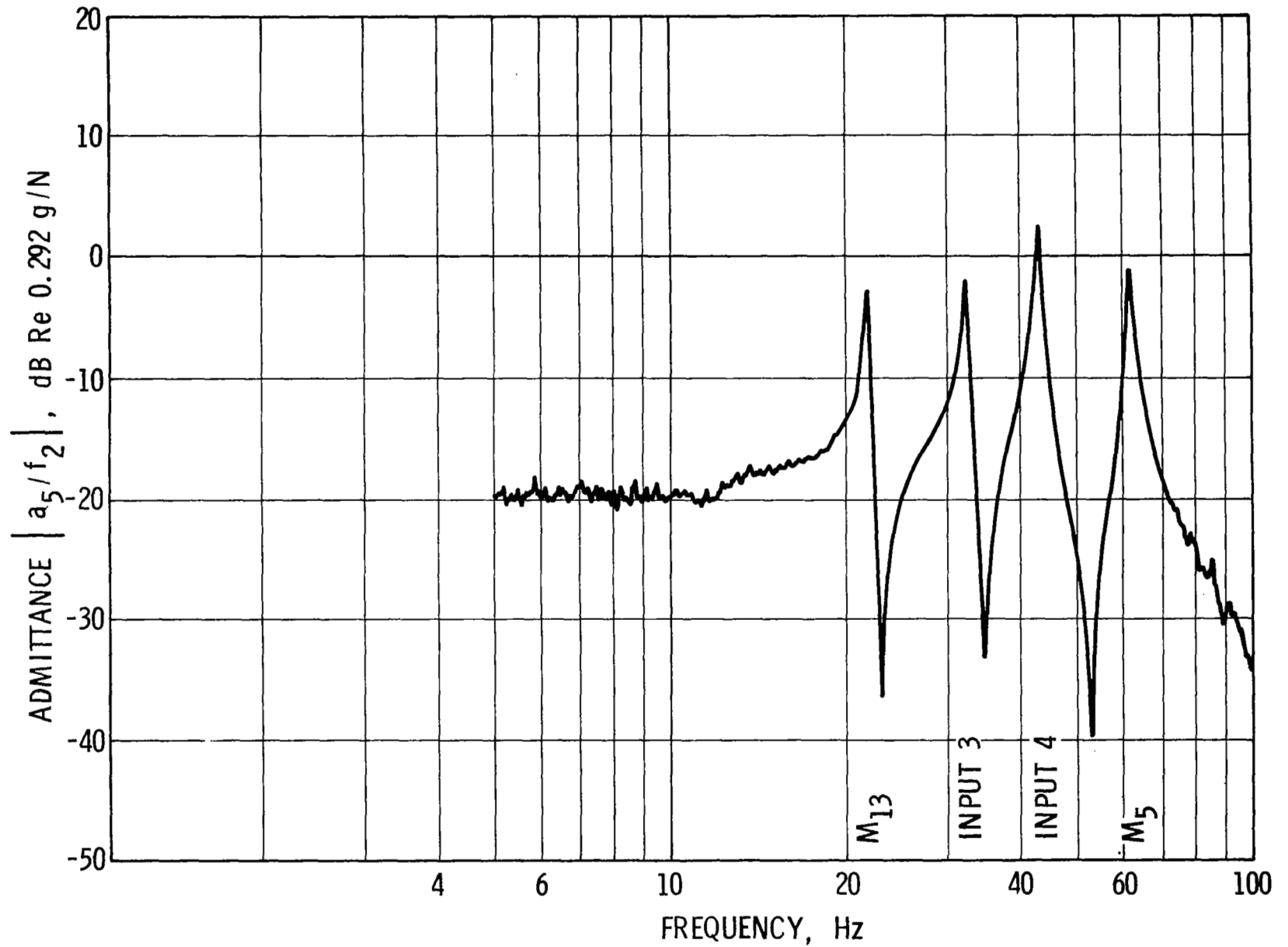26

Fig. 10. Experimental Response for Orbiter Model

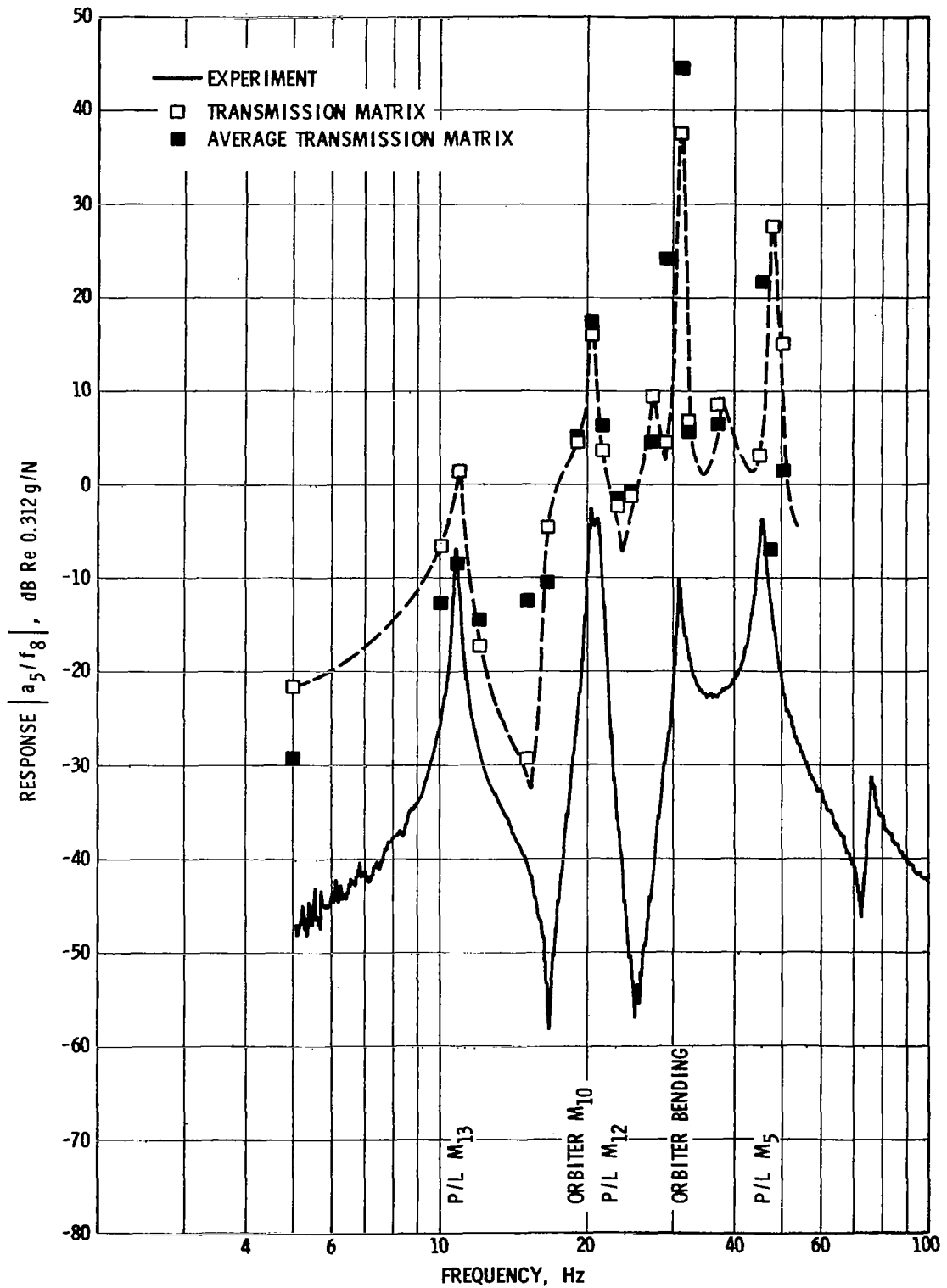Figure 11. Experimental Response for Flexible Payload

Figure 12. System Response with Flexible Payload Installed – Transmission Matrix Method

29

B.   Admittance Matrix Formulation

    1.   Flexible Payload Results

    Typical final results for the system with flexible payload installed are
given in Figure 13. Computed values are based on the use of Equation (17).
It is apparent that a reasonably acceptable comparison is achieved for this
method, and for most of the data, "as measured" or "averaged" results are
essentially the same. However, significant differences appear to result from
matrix nonsymmetry near resonance values. In some cases the nonsymmetry
was as much as 100%. These errors obviously reflect the extreme sensitivity
of the results near resonance to small differences in test conditions. The
dashed lines are drawn to show an extrapolation between the average admit-
tance values. Note that especially at resonant frequencies, sufficient resolu-
tions were not available in the predicted results to define completely the curve
peaks. Nevertheless, it appears that this method produces the best overall
correlation.

    Some results of attempts at error analysis are given in Figures 14
and 15. It was recognized that some noise level was present in the mea-
sured data. This was arbitrarily taken as 1/100 of the largest admittance
value present at a given frequency. All matrix elements below this value
were set equal to zero in both the payload and orbiter matrices, and final
results again computed. From Figure 14 it appears that this procedure
caused no significant difference in the final results.

    A second attempt at error analysis was conducted by deleting the
QUAD (or imaginary) value of admittance that occurred at 5 Hz. It is recog-
nized that at this frequency the motion of both components is essentially
that of a rigid body, and the admittances should be purely real numbers.
The 5-Hz value of QUAD as measured was considered error, and was de-
leted from all other values measured at other frequencies. The resulting
matrices were again used for prediction through Equation (17). Again,
however, significant differences in the results were not apparent, as can
be seen by comparing Figures 13 and 15.

    2.   Rigid Payload Results

    Figures 16 and 17 show final results for the system with rigid pay-
load installed. Measured orbiter admittance values and calculated payload
admittances were used in Equation (17) to produce the results shown in
Figure 16. It appears again that the averaged results produced the best
correspondence with the measured response values. Similar results occur
in Figure 17 for the measured rigid payload admittance values. However,
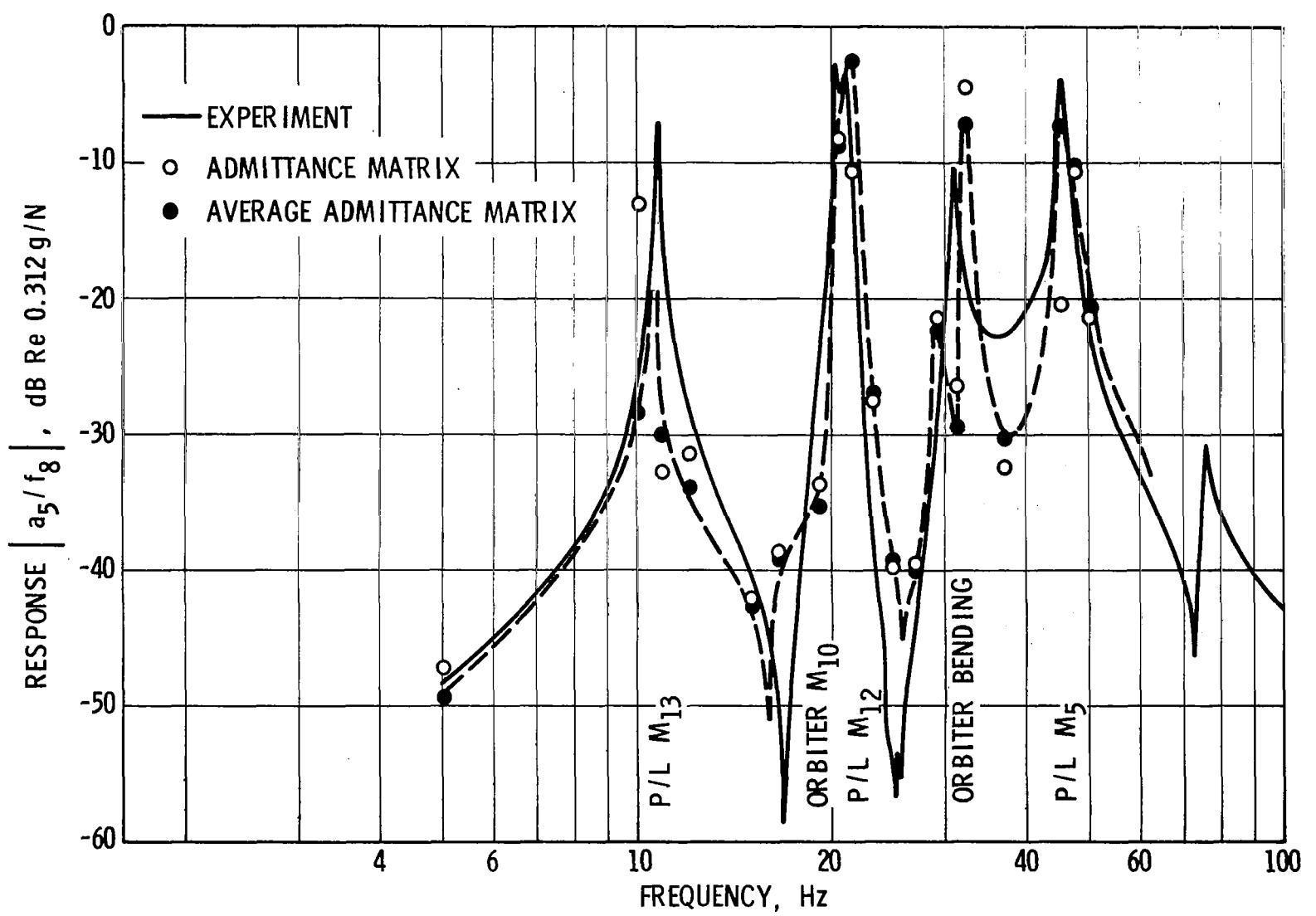here the points at 5 Hz and 37 Hz are significantly in error. Careful study

30

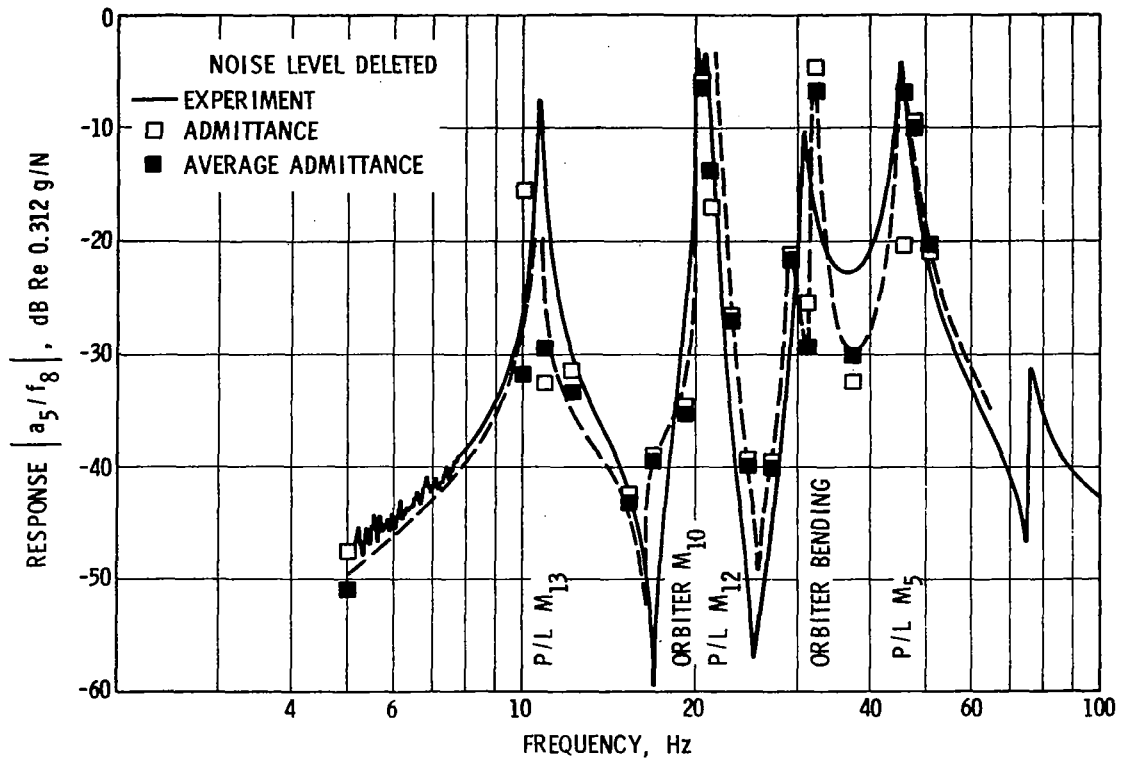Figure 13. System Response with Flexible Payload Installed – Admittance Matrix Method

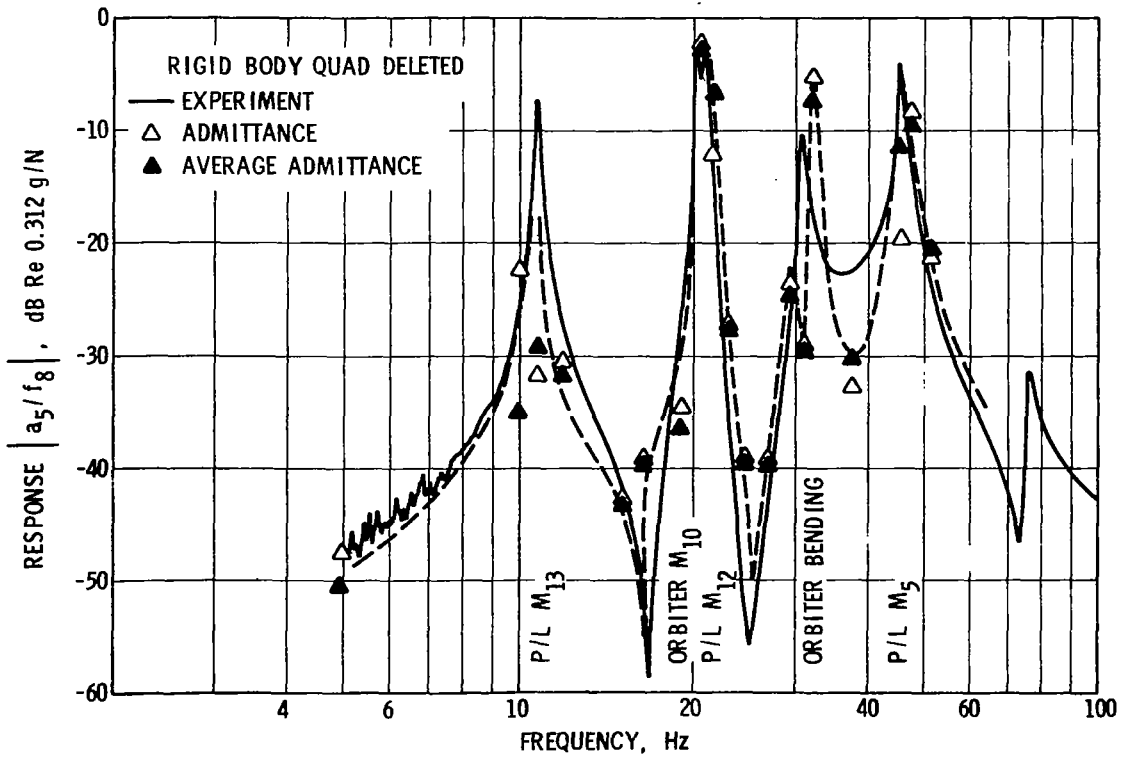Figure 14. Influence of Matrix Error on System Response

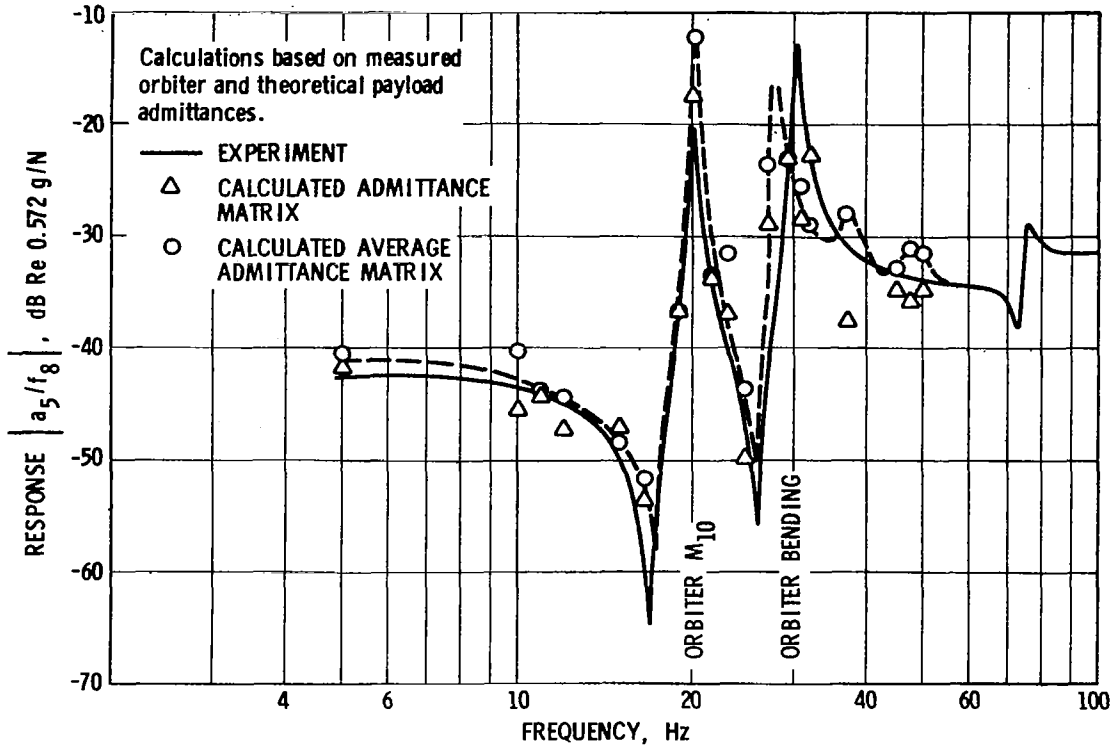Figure 15. Influence of Rigid Body Error on System Response

Figure 16. System Response with Rigid Payload Installed – Theoretical Payload Matrix
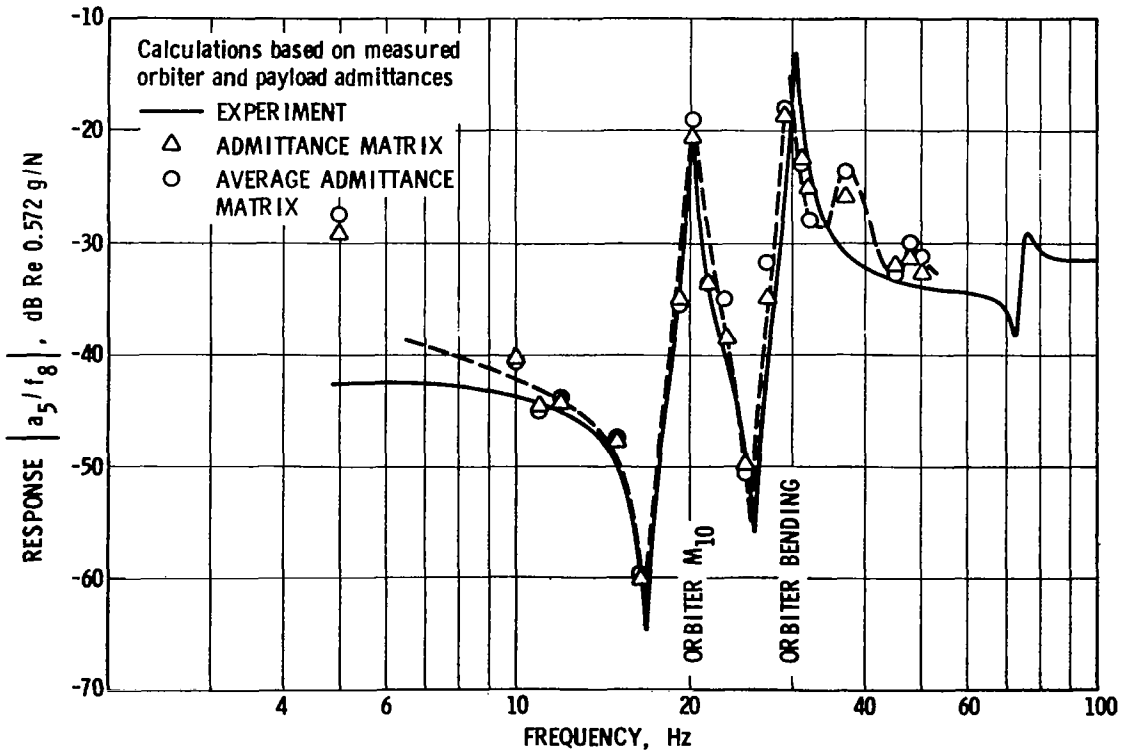

Figure 17. System Response with Rigid Payload Installed – Measured Matrix

33

of the data showed some 10% difference in some of the measured and theoretical admittance values at those frequencies. This error is magnified several times in the final results, as can be seen. Apparently the remaining discrepancy between measured and predicted system response is due to the error present in the measured orbiter admittance values, which are used to compute results for both Figures 16 and 17.

3. Flexible Payload Blocked Impedance Results

Sample results for some blocked impedances for the payload are shown in Figures 18 and 19, respectively. Various resonances are again identified. Final system results at the 19 discrete frequencies are shown in Figure 20. These results are based on the use of Equations (18) and (17). In general, these results appear to provide a somewhat better prediction between measured and predicted values, than was obtained in Figure 13 for the purely admittance matrix method. However, for the most part, the improvement is not significant. Thus, either admittance or blocked impedance techniques appear to produce a similar accuracy of prediction.
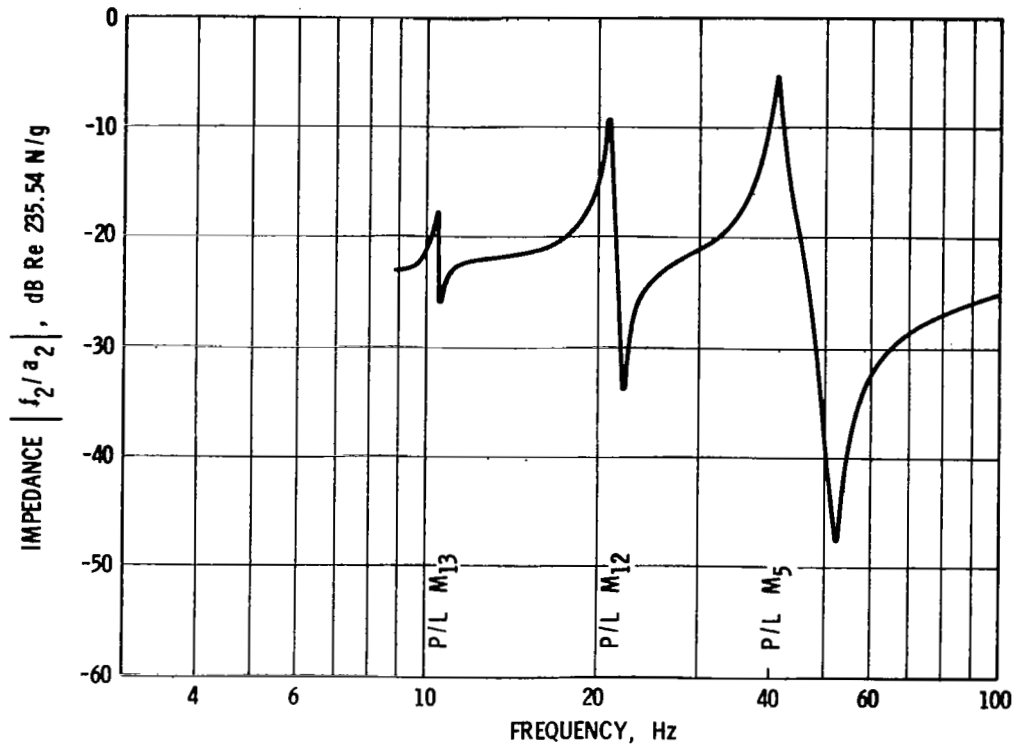
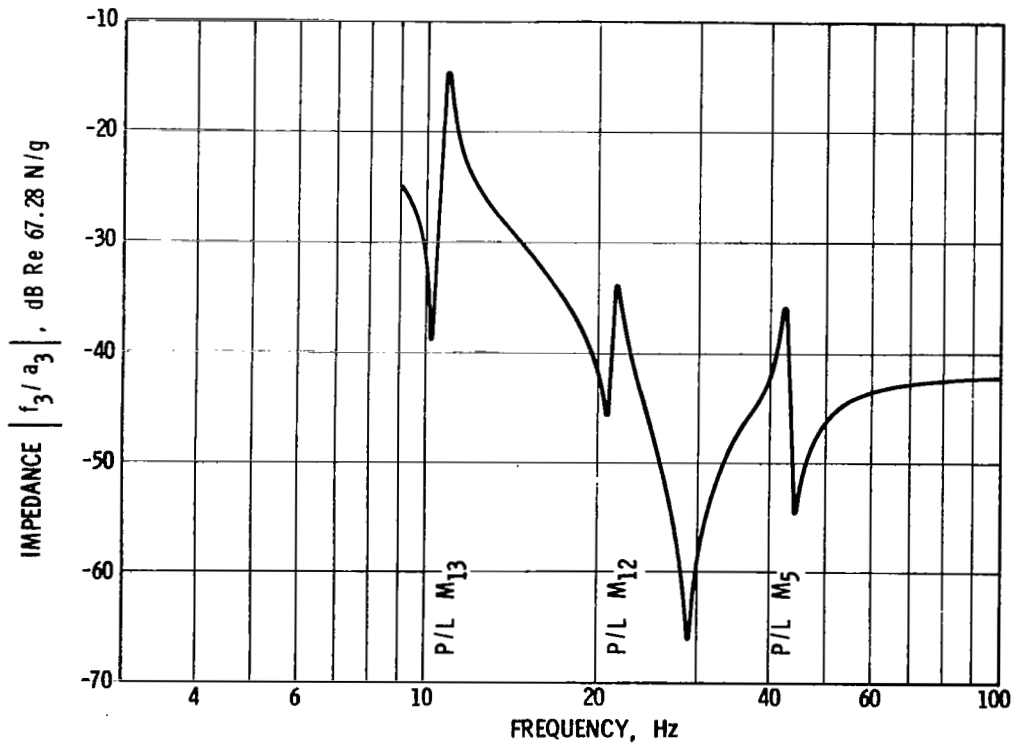Figure 18. Blocked Impedance Response for Flexible Payload – Excitation at F_2

Figure 19. Blocked Impedance Response for Flexible Payload – Excitation at F_3
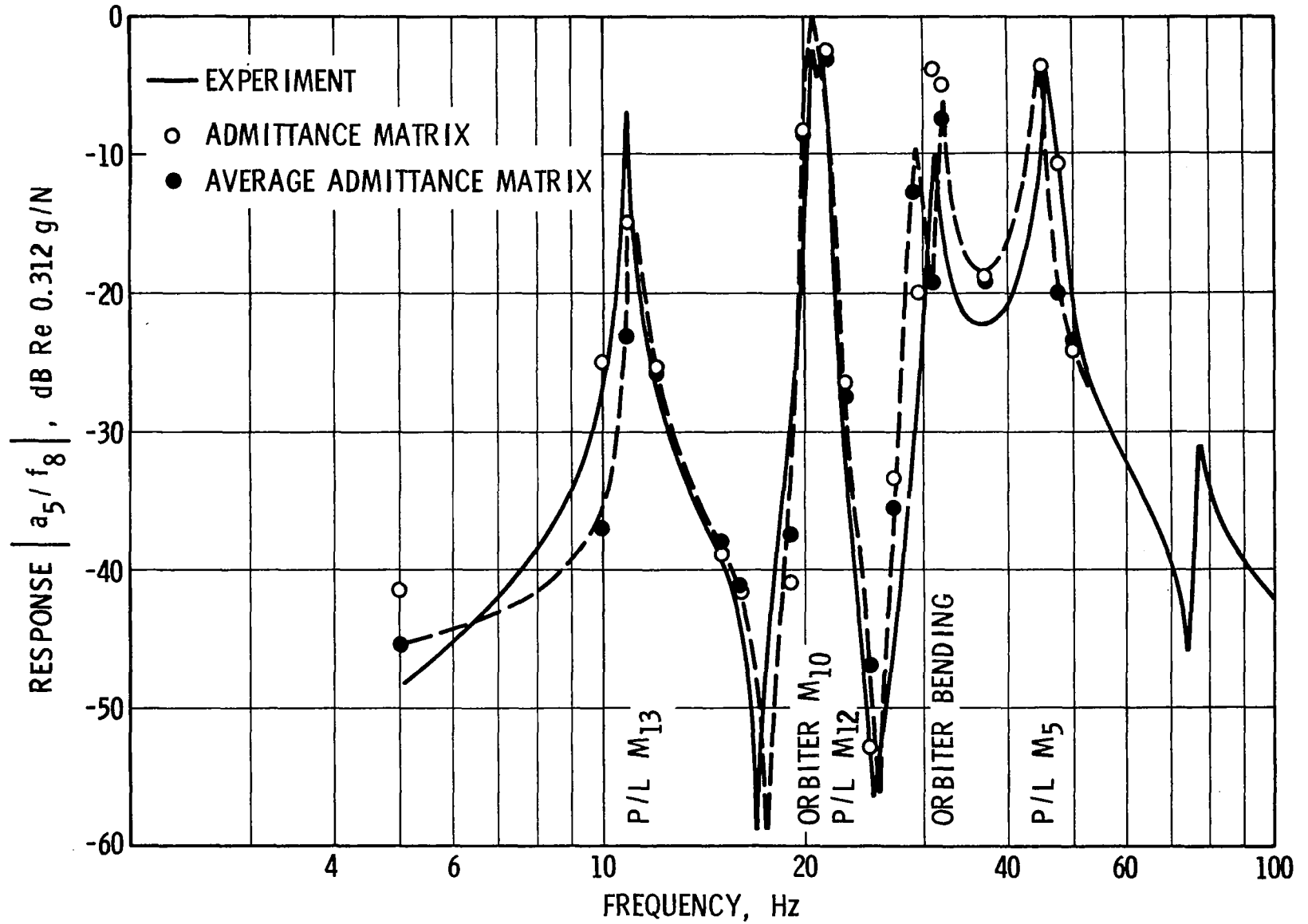
35

Figure 20. System Response with Flexible Payload – Blocked Impedance Results

V. CONCLUSIONS

In view of the preceding results and implications, several positive conclusions can be identified from this study.

1. The transmission matrix method is undesirable for prediction of payload responses in the combined system if measured component parameters are to be utilized.

2. The admittance matrix method produces a satisfactory prediction of payload responses under similar input conditions. It also requires fewer measurements than the transmission matrix method.

3. Use of forced symmetry by averaging off-diagonal admittance elements is desirable.

4. Noise error of the order of 1/100 the maximum measured values at a given frequency have no effect on the final results.

5. Simulated free-free admittance or fixed boundary blocked impedance tests for the payload appear to produce similar accuracy in prediction.

6. Use of steady-state sinusoidal procedures for data acquisition is extremely cumbersome and time-consuming. For practical application of these techniques a far more rapid and automated data acquisition process will be required.

REFERENCES

1. Klosterman, A. L., and Lemon, J. R., "Dynamic Design Analysis Via the Building Block Approach, " Shock and Vibration Bulletin No. 42, Part 1, pp. 97-104.

2. Flannelly, W. G., Berman, A., and Barnsby, R. M., "Theory of Structural Dynamic Testing Using Impedance Techniques, " USAAVLABS Technical Report 70-6A, Vol. I, Theoretical Development, June 1970.

3. Rubin, S., "Transmission Matrices for Vibration and Their Relation to Admittance and Impedance, " ASME Transactions, Journal of Engineering for Industry, Vol. 86, Series B, No. 1, (1964), pp. 9-21.

4. Noiseux, D. U., and Meyer, E. B., "Application of Impedance Theory and Measurements to Structural Vibration, " AFFDL-TR-67-182, August 1968.